

## Article

# Photodynamic Polymers Constituted by Porphyrin Units as Antibacterial Materials

María B. Ballatore<sup>1</sup>, María E. Pérez<sup>1</sup> , Sofía C. Santamarina<sup>1</sup>, Javier E. Durantini<sup>2</sup>, María E. Milanesio<sup>1</sup> and Edgardo N. Durantini<sup>1,\*</sup> 

<sup>1</sup> IDAS-CONICET, Departamento de Química, Facultad de Ciencias Exactas, Físico-Químicas y Naturales, Universidad Nacional de Río Cuarto, Ruta Nacional 36 Km 601, Río Cuarto X5804BYA, Argentina

<sup>2</sup> IITEMA-CONICET, Departamento de Química, Facultad de Ciencias Exactas, Físico-Químicas y Naturales, Universidad Nacional de Río Cuarto, Ruta Nacional 36 Km 601, Río Cuarto X5804BYA, Argentina

\* Correspondence: edurantini@exa.unrc.edu.ar

**Abstract:** Photodynamic inactivation of microorganisms has emerged as a promising strategy to kill and eradicate pathogens. In this work, two polymers, **TCP-P** and **ZnTCP-P**, were synthesized by oxidative polymerization of 5,10,15,20-tetrakis [3-(*N*-ethylcarbazoyl)]porphyrin and its complex with Zn(II). Solid polymers consist of rods (diameter 100 nm, length ~100–500 nm) that form microporous structures on a surface. UV-visible absorption spectra in solution showed the Soret and Q bands characteristic of the corresponding constitutional porphyrins. In addition, the polymers presented two red emission bands with quantum yields  $\Phi_F = 0.11$  for **TCP-P** and  $\Phi_F = 0.050$  for **ZnTCP-P**. These compounds sensitized the production of singlet molecular oxygen with quantum yields of  $\Phi_{\Delta} \sim 0.3$ . Thus, the spectroscopic and photodynamic properties of the porphyrin units were maintained in the conjugates. The photodynamic activity induced by both polymers was tested to inactivate *S. aureus*. In cell suspensions, **TCP-P** was more effective than **ZnTCP-P** in killing bacteria. Viable *S. aureus* cells were not detected using 4  $\mu\text{M}$  **TCP-P** after 20 min of irradiation. Moreover, both polymers showed a high photocytotoxic activity to eradicate *S. aureus* cells attached to a surface. The results indicate that these conjugated polymers can act as effective antimicrobial agents to photoinactivate pathogens.

**Keywords:** porphyrin; polymer; singlet oxygen; photodynamic inactivation; antimicrobial



**Citation:** Ballatore, M.B.; Pérez, M.E.; Santamarina, S.C.; Durantini, J.E.; Milanesio, M.E.; Durantini, E.N. Photodynamic Polymers Constituted by Porphyrin Units as Antibacterial Materials. *Photochem* **2022**, *2*, 891–904. <https://doi.org/10.3390/photochem2040057>

Academic Editor: Detlef W. Bahnemann

Received: 10 September 2022

Accepted: 24 October 2022

Published: 9 November 2022

**Publisher's Note:** MDPI stays neutral with regard to jurisdictional claims in published maps and institutional affiliations.



**Copyright:** © 2022 by the authors. Licensee MDPI, Basel, Switzerland. This article is an open access article distributed under the terms and conditions of the Creative Commons Attribution (CC BY) license (<https://creativecommons.org/licenses/by/4.0/>).

## 1. Introduction

Antimicrobial resistance is continually increasing while the development of new drugs for conventional use is running out. Therefore, many bacterial infections that were previously relatively easy to cure are becoming untreatable diseases [1]. Pharmaceutical products have allowed improvement in many specialties of medical practice. Successful outcomes of surgical procedures and various immunosuppressive therapies depend on antibiotic prophylaxis. However, in many cases, the inappropriate use of antimicrobials has led to a considerable increase in bacterial resistance, denoting a permanent threat to public health worldwide [2].

Although diseases can be caused by a wide variety of microorganisms, bacteria are responsible for the main infections acquired in hospitals and health care centers [3]. The Gram-positive bacterium *Staphylococcus aureus* is considered one of the pathogens that has developed the greatest epidemiological resistance [4]. The appearance of methicillin-resistant *S. aureus* (MRSA) has become an important therapeutic challenge to remedy the infections caused by this pathogen [5]. The antibiotic resistance developed by MRSA poses a major threat to global health care. MRSA infections increase the risk of death and the cost of treatment for patients. Many hospital-acquired infections are caused by MRSA, posing a high risk to patients. Contaminated objects that come into contact with healthcare workers and patients represent the greatest risk of pathogen colonization and nosocomial infections [6]. Moreover, the considerable transmission of MRSA can occur in household

settings from patients infected or colonized with this pathogen to their domestic contacts [4]. Therefore, it is relevant to develop possible therapies that replace or complement the use of conventional antibiotics to cure infections caused by resistant pathogens [7].

Among the alternative therapies, photodynamic inactivation (PDI) of pathogens represents an interesting approach to eliminating resistant microbial cells [8]. Essentially, this methodology is based on the addition of a photosensitizer (PS), which selectively interacts with microorganisms. Irradiation of microbes with the light of appropriate wavelengths in the presence of oxygen results in the formation of reactive oxygen species (ROS). These intermediates can react with various cellular components in the vicinity of where they were generated. These changes produce a loss of functionality in cellular constituents, leading to microbial inactivation. Two photodynamic pathways sensitized by the PS are mainly involved in PDI therapy [9]. In the type I mechanism, the PS excited triplet state reacts with biological molecules by electron or proton transfer generating free radicals, which can react with oxygen to produce ROS. On the other hand, the PS excited triplet state can produce energy transfer to oxygen forming singlet molecular oxygen,  $O_2(^1\Delta_g)$ , which is known as the type II process [10]. Unlike traditional antibiotics, PSs generate ROS that can cause cytotoxic damage to a wide variety of microbial biomolecules that are lethal to cells. Therefore, at this time, the chances of microbes developing resistance to PDI are considered very improbable [11].

Tetrapyrrolic macrocycle derivatives represent one of the most studied families of PSs for PDI [12,13]. Generally, these compounds present a high aggregation in aqueous media that contain microorganisms. This drawback limits the full application of these PSs in PDI. The substitution in the periphery of the macrocycle by groups that allow the improvement of the interaction with the microbial cells is a possibility for potential medical applications [12,13]. However, another alternative is to form conjugated polymers consisting of porphyrin units that allow improving the photoinactivating capacity of bacteria [14,15].

In the present study, 5,10,15,20-tetrakis[3-(*N*-ethylcarbazoyl)]porphyrin (TPC) and its complex with Zn(II) (ZnTPC) were used as the modular unit to obtain the conjugated polymers TCP-P and ZnTCP-P, respectively. In a previous investigation, electrogenerated polymeric films of these porphyrins were formed on optically transparent indium tin oxide (ITO) electrodes [16,17]. These films were proposed as antimicrobial materials to obtain aseptic conditions. Herein, polymers obtained in the solution were first examined for shape and size by scanning electron microscopy (SEM). In order to use these compounds as photosensitizing agents in PDI, the spectroscopic characteristics and photodynamic properties of these polymeric materials were determined in solution and compared with those of their constitutional porphyrins. In addition, the photoinactivating ability sensitized by these polymers was evaluated in MRSA cell suspensions and in bacterial cells adhered to surfaces in order to establish their antimicrobial activities activated by visible light.

## 2. Materials and Methods

Chemicals and instrumentation are detailed in Supplementary Materials.

### 2.1. Synthesis of PSs

TCP and ZnTCP were obtained as previously reported with some modifications [16,17].

**TCP.** A solution of *N*-ethyl-3-carbazolecarbaldehyde (892 mg, 4.0 mmol) and pyrrole (295  $\mu$ L, 4.25 mmol) in 400 mL of dichloromethane was purged with argon for 2 h. Then, trifluoroacetic acid (315  $\mu$ L, 4.25 mmol) was added, and the solution was stirred for 60 min at room temperature. Then, 2,3-dichloro-5,6-dicyano-1,4-benzoquinone (DDQ, 1.26 g, 4.25 mmol) was added, and the mixture was stirred for 6 h, open to the atmosphere at room temperature. The solvent was removed under reduced pressure, and flash column chromatography (silica gel, dichloromethane/triethylamine 1%) afforded 282 mg (26%) of pure TCP. TLC (silica gel, dichloromethane/triethylamine 1%)  $R_f = 0.65$ . Spectroscopic data of TCP coincide with those previously reported [16].

**ZnTCP.** A solution of **TCP** (60 mg, 0.054 mmol) in 50 mL of dichloromethane was treated with 5 mL of a saturated solution of Zn(II) acetate in methanol. The mixture was stirred for 5 h at room temperature. The reaction progress was monitored by UV-visible absorption. Then, the reaction mixture was treated with water (25 mL), and the organic phase was extracted with three portions of dichloromethane (25 mL each). The organic solvents were evaporated under reduced pressure yielding 59 mg (96%) of pure **ZnTCP**. TLC (silica gel, dichloromethane/triethylamine 1%)  $R_f = 0.60$ . Spectroscopic data agree with those previously reported [17].

**TCP-P.** The synthesis of this polymer was carried out by means of an oxidative reaction with  $\text{FeCl}_3$  [18]. **TCP** (54 mg, 0.050 mmol) was dissolved in anhydrous chloroform (10 mL). Then, a solution of dry  $\text{FeCl}_3$  (4:1 molar ratio to porphyrin) in chloroform was added. The mixture was vigorously stirred for 8 h at room temperature and under an argon atmosphere. The progress of the reaction was analyzed by TLC (silica gel, dichloromethane/triethylamine 1%). The **TCP** spot disappears while the product is retained at the origin. After that, the solvent was removed under reduced pressure, and the solid was resuspended in methanol (10 mL). The polymer was separated by centrifugation (15 min, 3000 rpm), and the supernatant was removed. The solid was washed three times (5 mL each) with methanol and recentrifuged. The precipitate obtained was dried under vacuum to obtain 44 mg (81%) of **TCP-P** (Figure S1).

**ZnTCP-P.** This polymer was obtained using the methodology described above for **TCP-P** from **ZnTCP** (47 mg, 0.041 mmol) to yield 39 mg (83%) of **ZnTCP-P**. TLC (silica gel, dichloromethane/triethylamine 1%) analysis indicated that the **ZnTCP-P** spot disappears, and the product spot is retained at the origin.

## 2.2. Spectroscopic Determinations

UV-visible absorption and fluorescence emission spectra were achieved in *N,N*-dimethylformamide (DMF) at room temperature using a quartz cell of 1 cm path length. Fluorescence emission spectra were determined by exciting the solutions at 435 nm. The absorbances of the samples were 0.05 at the excitation wavelength. Emission spectra were integrated in the range between 575 and 800 nm. The fluorescence quantum yield ( $\Phi_F$ ) of the PSs was determined by comparing the area under the emission spectrum, using **TCP** as a reference ( $\Phi_F = 0.12$  in DMF) [19].

## 2.3. Photooxidation of 9,10-dimethylantracene (DMA)

DMA (35  $\mu\text{M}$ ) and PS ( $A = 0.1$  at 430 nm) were dissolved in 2 mL of DMF. Samples were irradiated with light at 430 nm (0.38  $\text{mW}/\text{cm}^2$ ). The photooxidation rate of DMA was investigated by analyzing the decrease in absorbance at 379 nm. The observed rate constant of DMA decomposition ( $k_{\text{obs}}^{\text{DMA}}$ ) for each PS was obtained from the pseudo-first-order kinetic plot of  $\ln(A_0/A)$  vs. time. The quantum yield values of  $\text{O}_2(^1\Delta_g)$  production ( $\Phi_\Delta$ ) were calculated by comparing the  $k_{\text{obs}}^{\text{DMA}}$  for each PS with that for **TCP**, which was used as a reference ( $\Phi_\Delta = 0.41$  in DMF), under the same experimental conditions [19].

## 2.4. *S. aureus* Strain and Growth Conditions

Bacterial cultures of MRSA (ATCC 43300) were preserved in glycerol 10% (*v/v*) and tryptic soy (TS) broth 90% (*v/v*) at  $-80^\circ\text{C}$ . A bacterial strain was grown in TS agar at  $37^\circ\text{C}$  overnight. After that, 400  $\mu\text{L}$  of the culture was aseptically transferred to 4 mL of fresh TS broth. The cells were incubated at  $37^\circ\text{C}$  until the exponential phase of growth was obtained ( $A = 0.4$  at 660 nm). Cells were collected by centrifugation (3000 rpm for 15 min) and re-suspended in 4 mL of PBS, which corresponds to a cell density of  $\sim 10^8$  colony-forming units (CFU)/mL. Then, this cell suspension was diluted in PBS to obtain  $\sim 10^4$  CFU/mL. The number of viable bacteria was determined by the spread plate technique using 10-fold serial dilutions in PBS. Each cell suspension was plated on TS agar plates in triplicate. Colony formation was quantified after incubating the plates for 24 h at  $37^\circ\text{C}$  in the dark [15].

### 2.5. Photosensitized Inactivation of *S. aureus* Cell Suspensions

*S. aureus* cell suspensions (2 mL,  $\sim 10^4$  CFU/mL in PBS) in Pyrex culture tubes (13 × 100 mm) were treated with 2 and 4  $\mu\text{M}$  PS for 30 min in the dark at 37 °C. Stock solutions of PSs (0.5 mM) were prepared in DMF, which were used to add the PS to the cultures. An aliquot (200  $\mu\text{L}$ ) of each culture was transferred to 96-well microtiter plates, which were irradiated with white light (90 mW/cm<sup>2</sup>) at different times (10, 20, and 30 min) [20]. Viable cells were quantified as detailed above.

### 2.6. Photoinactivation at the Single-Bacterium Level

Fluorescence microscopy investigations were performed according to the reported methodology [21]. For this, *S. aureus* cells were aerobically grown in TS agar for 18 h at 37 °C. Then, a single colony was selected and cultured overnight in TS agar. Bacteria were collected from the agar by adding 1 mL of PBS and removing the agar streaks. After that, *S. aureus* suspension (1 mL) was incubated in a chamber composed of a polymeric cylinder glued to a coverslip for 30 min at 37 °C. This process is used for bacterial cells to adhere to the glass surface. The chamber was washed with PBS to remove unbound bacteria. Bioimaging experiments were performed by adding 583  $\mu\text{L}$  of PBS and propidium iodide (1  $\mu\text{M}$ ) to cells adhered to the glass surface of the chamber. *S. aureus* cells were incubated for 15 min in the dark. Then, the PS was added (4  $\mu\text{M}$ ), and the bacteria were incubated for another 20 min in the dark. The chamber was irradiated with green light using a bandpass filter (525/35) measured out of the objective (1.0 mW/cm<sup>2</sup>). Fluorescence images of PI were obtained using an emission band pass filter (645/75). For each imaging region, a brightfield image was acquired to check bacterial cells. Images were collected using a 100× magnification objective and captured by a CMOS camera.

### 2.7. Statistical Analysis

*S. aureus* controls were achieved using irradiated cells without the PS and in the presence of PS in the dark. Three separate experiments were used to determine each reported value. Error bars represent standard deviations. Statistically significant values were determined by one-way ANOVA, considering a confidence level of 95% ( $p < 0.05$ ).

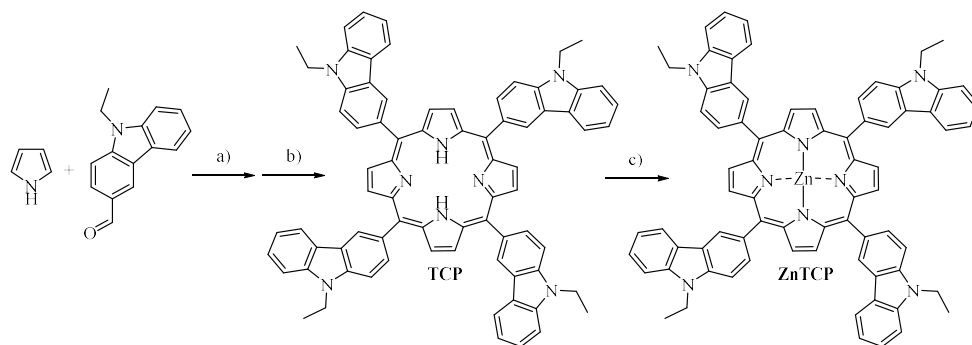
## 3. Results and Discussion

### 3.1. Synthesis of TCP-P and ZnTCP-P

The synthetic approach to obtain TCP monomer containing carbazoyl groups is shown in Scheme 1. The condensation catalyzed by the acid of *N*-ethyl-3-carbazolecarbaldehyde and pyrrole was carried out in dichloromethane at room temperature for 2 h. This procedure yielded the porphyrinogen macrocycle, which was oxidized with DDQ and gave rise to porphyrin TCP in 26% yield as a purple solid after a simple purification by flash column chromatography. This free-base porphyrin was then metalated by treating TCP with Zn(II) acetate in dichloromethane/methanol at room temperature to give the desired metal complex ZnTCP in 96% yield. These methods produce appropriated yields of the free-base and Zn(II) metalized porphyrins substituted by four carbazoyl residues at the periphery of the macrocycle.

The synthesis of TCP-P and ZnTCP-P was carried out by means of an oxidative polymerization with FeCl<sub>3</sub> [18,22]. In both porphyrins, the group that has the ability to polymerize is the carbazole after the formation of the cation radical. Carbazole oxidation is known to lead to the dimerization of two radical cations through the 3,3'-positions [23]. Scheme 2 shows the synthetic procedure to obtain polymeric compounds. In this approach, porphyrin was dissolved in anhydrous chloroform. A solution of anhydrous FeCl<sub>3</sub> in chloroform was added dropwise to this solution, which was kept under vigorous stirring. The progress of the reaction was tested by TLC, indicating that the porphyrin spot completely disappears while a spot appears due to the formation of the polymer, which is retained in the seeding site. These spots showed red emission when irradiated with UV light. In addition, the UV-visible absorption spectrum of the reaction mixture presented a band

centered at 477 nm (Figure S2), which is consistent with that of the polymer in the oxidized state and was previously attributed to the formation of dicarbazole units [16]. The solvent was evaporated, the solid was resuspended in methanol, and the polymer was separated by centrifugation. In order to avoid free porphyrin residues, the precipitate was purified by being washed with methanol (Figure S1). The precipitate finally obtained was dried under vacuum to yield 81% **TCP-P** and 83% **ZnTCP-P**. In both cases, the desired products were obtained quickly and easily from the corresponding porphyrins. Figure 1 depicts an idealized three-dimensional configuration where the spatial arrangement of seventeen porphyrin monomers can be observed.



**Scheme 1.** Synthesis of TCP and ZnTCP. Reagents and conditions: a) trifluoroacetic acid, dichloromethane, r.t., 2 h; b) DDQ, dichloromethane, r.t., 6 h, 26%; c)  $\text{Zn}(\text{CH}_3\text{COO})_2$ , dichloromethane/methanol, 8 h, 96%.

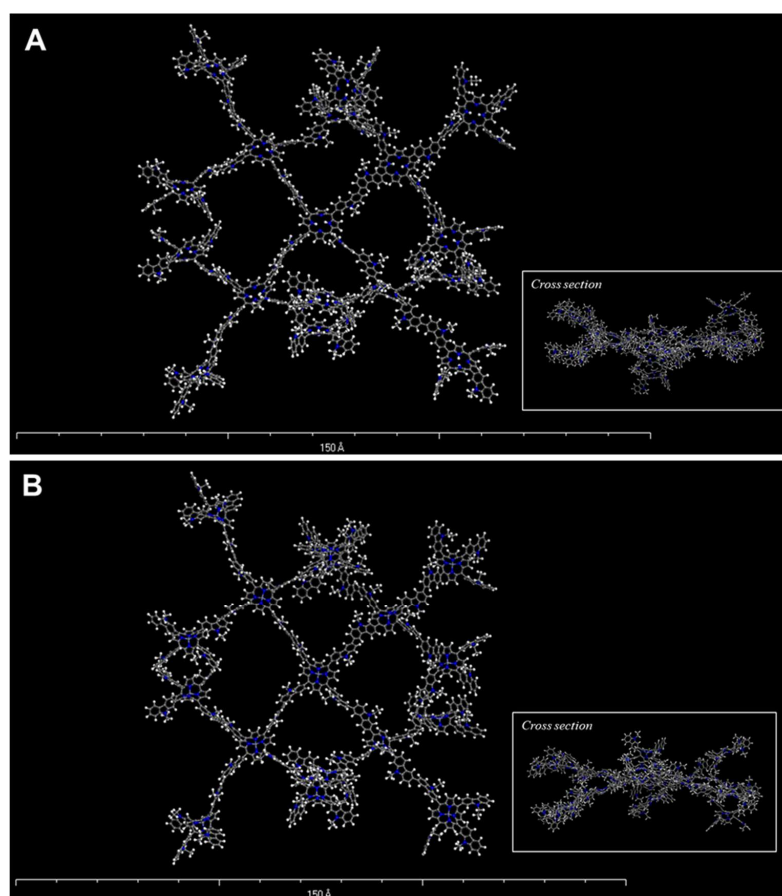
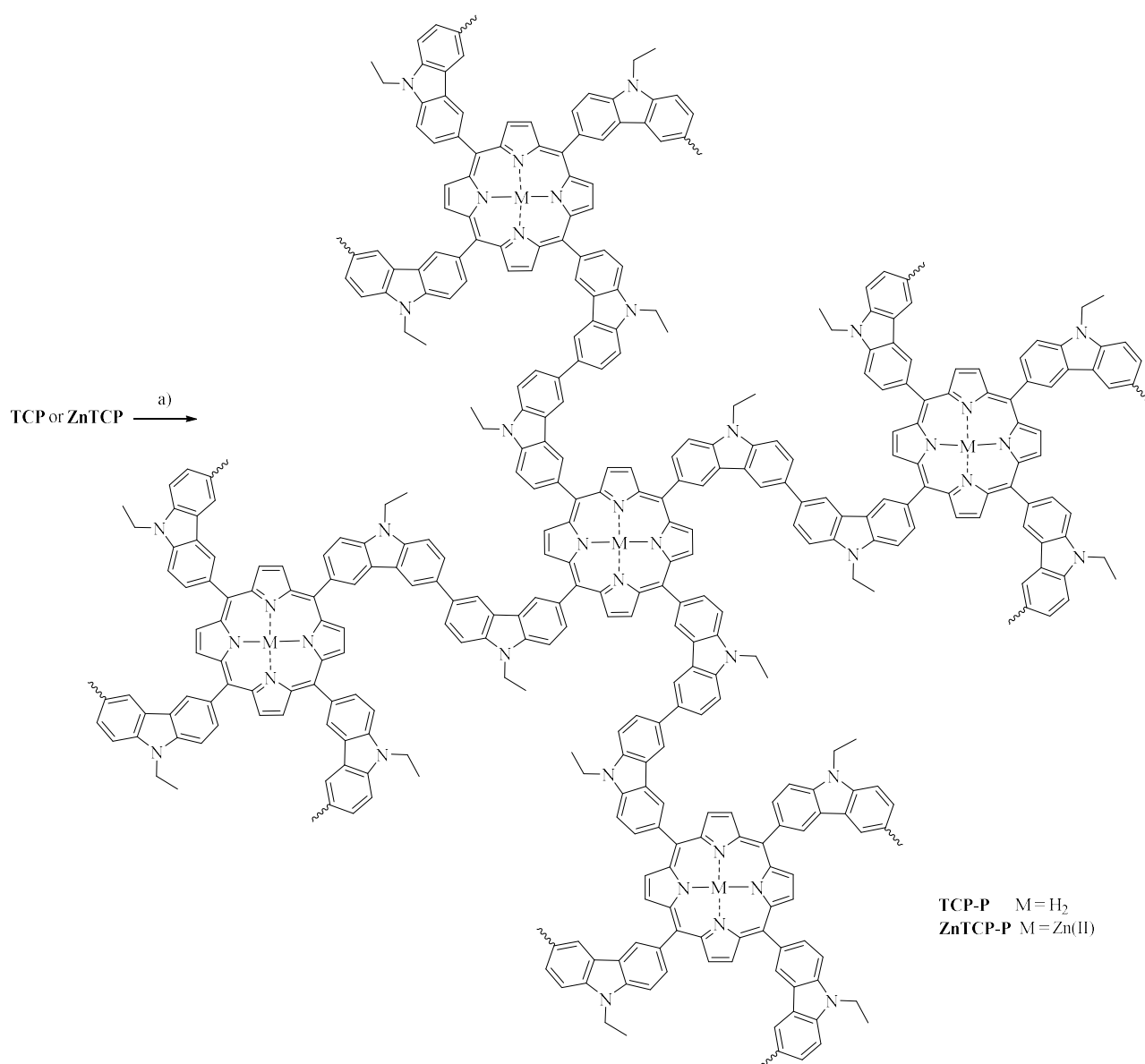


**Figure 1.** Idealized three-dimensional configuration of seventeen porphyrin monomers corresponding to (A) **TCP-P** and (B) **ZnTCP-P**. The geometry of the proposed structures was optimized using the Forcite molecular mechanic module. Insets: cross-section of the simulated polymers.





**Scheme 2.** Synthesis of TCP-P and ZnTCP-P. Reagents and conditions: a) FeCl<sub>3</sub>, chloroform, r.t., 8 h, 81% TCP-P and 83% ZnTCP-P.

### 3.2. SEM Images of the Polymer

The conjugated polymers TCP-P and ZnTCP-P were examined by SEM images with the aim of evaluating the shape, distribution, and porosity of the polymers formed. Thus, an aliquot of the polymer in chloroform was spread on a glass surface of a slide. The solvent was evaporated in a vacuum at room temperature to obtain a film. Figure 2 exhibits representative SEM images of these materials. TCP-P and ZnTCP-P polymers present the shape of rods, with a diameter of about 100 nm and a length distribution between 100 and 500 nm. In addition, the SEM images show a complete coating of the glass surface with polymers, which form microporous structures on the surface. The porous material allows for obtaining a larger contact surface, which is convenient for improving the PDI of bacteria [15]. Similar structures were previously found for polymers of porphyrins and fullerene C<sub>60</sub> [24]. It was supposed that the superstructures of these assemblies were constructed by the intermolecular  $\pi$ - $\pi$  interaction.

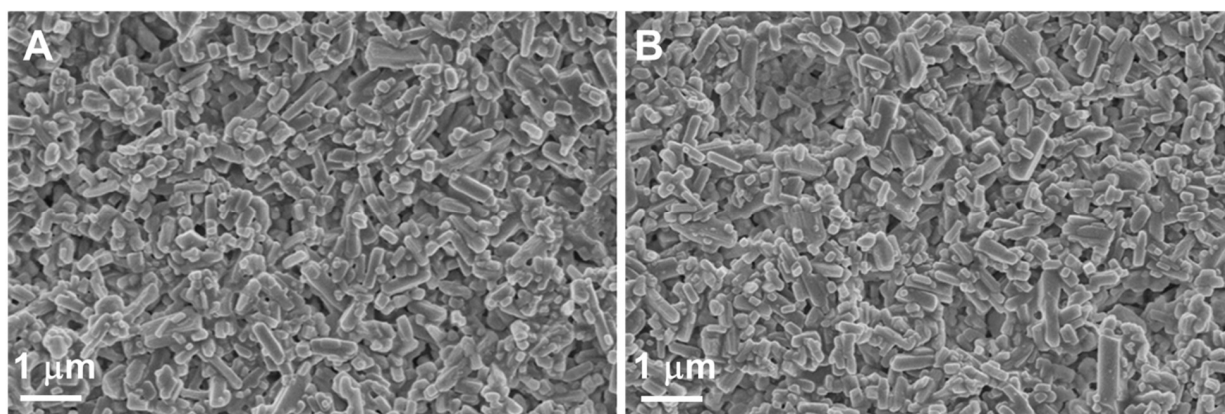


**Figure 2.** SEM images of (A) TCP-P and (B) ZnTCP-P deposited as a film on glass.

### 3.3. Spectroscopic Characterization

The optical properties of TCP-P and ZnTCP-P were compared with their corresponding monomers in DMF. Figure 3A shows the UV-visible absorption spectra. The spectroscopic characteristics of these PSs are summarized in Table 1. The spectra of the monomers TCP and ZnTCP exhibit a Soret band at  $\sim 430$  nm with a high molar absorption coefficient ( $10^5$  Lmol $^{-1}$ cm $^{-1}$ ). TCP presents four Q-bands between 515 and 650 nm, which involved the transitions  $Q_x(0,0)$ ,  $Q_x(1,0)$ ,  $Q_y(0,0)$ , and  $Q_y(1,0)$  associated with a  $D_{2h}$  symmetry [25]. In contrast, ZnTCP has two Q bands between 550 and 620 nm. These bands are representative of the complex of Zn(II) with *meso*-substituted porphyrins [26,27]. The absorption spectra of TCP-P and ZnTCP-P indicate that the spectroscopic properties of the corresponding porphyrin units were preserved in the polymers, even when they are forming a largely conjugated system. The absorption bands of TCP-P and ZnTCP-P are slightly bathochromically shifted compared to TCP and ZnTCP, respectively. In both cases, the peaks of the Soret bands showed a red shift of 6 nm. These shifts are accompanied by a broadening of the bands in the polymers, which may be due to a small interaction between the porphyrin units in the conjugated structure [15].

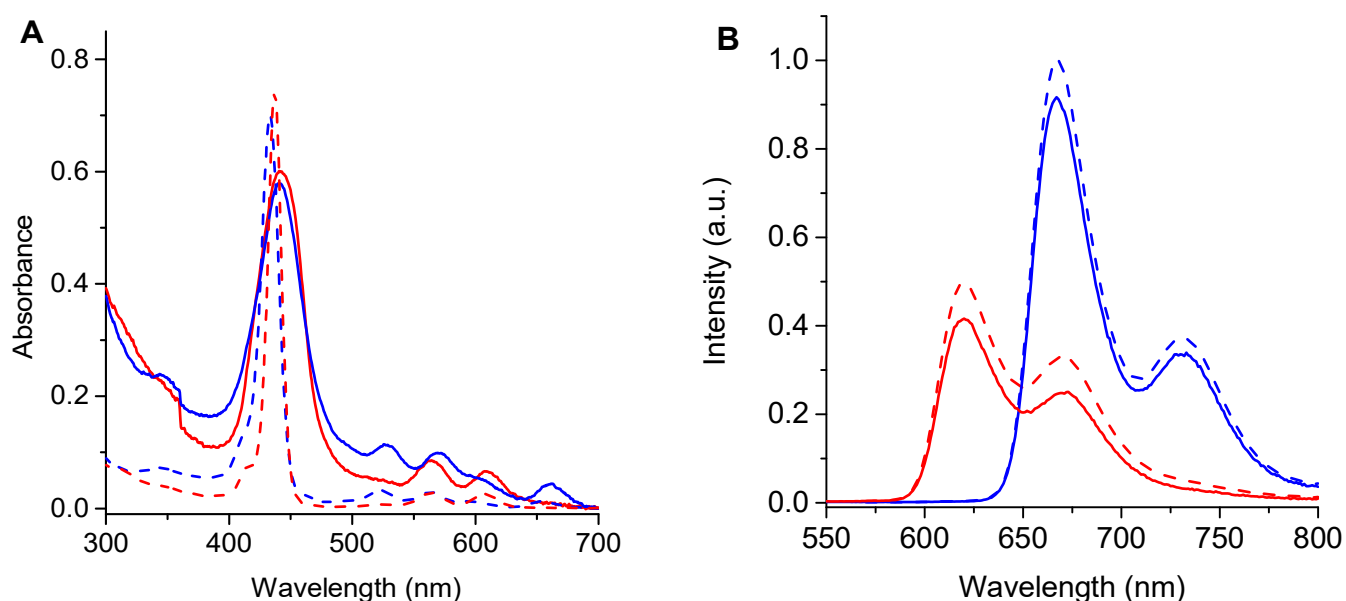


**Figure 3.** (A) UV-visible absorption and (B) fluorescence emission spectra of TCP (blue dashed line), ZnTCP (red dashed line), TCP-P (blue solid line), and ZnTCP-P (red solid line) in DMF ( $\lambda_{exc} = 435$  nm).

**Table 1.** Spectroscopic and photodynamic properties of PSs in DMF.

PS	$\lambda^{\text{Soret}}$ (nm)	$\epsilon^{\text{Soret}}$ a	$\lambda_{\text{em}}$ (nm)	$\Phi_{\text{F}}$ b	$k_{\text{obs}}^{\text{DMA}}$ (s <sup>-1</sup> ) c	$\Phi_{\Delta}$ d
TCP	434	$2.81 \times 10^5$	667	$0.12 \pm 0.01$	$(2.09 \pm 0.02) \times 10^{-4}$	$0.41 \pm 0.02$
ZnTCP	437	$2.98 \times 10^5$	620	$0.060 \pm 0.002$	$(2.24 \pm 0.02) \times 10^{-4}$	$0.44 \pm 0.02$
TCP-P	440	-	667	$0.11 \pm 0.01$	$(1.80 \pm 0.01) \times 10^{-4}$	$0.33 \pm 0.01$
ZnTCP-P	443	-	620	$0.050 \pm 0.002$	$(1.67 \pm 0.01) \times 10^{-4}$	$0.31 \pm 0.01$

a Molar absorption coefficient (Lmol<sup>-1</sup>cm<sup>-1</sup>), b fluorescence quantum yield, c observed rate constants for the photooxidation reaction of DMA, d quantum yield of O<sub>2</sub>(<sup>1</sup>Δ<sub>g</sub>) production.

Fluorescence emission spectra of TCP-P and ZnTCP-P in DMF are shown in Figure 3B. The monomers presented two bands centered at 667 and 730 nm for TCP and 620 and 670 nm for ZnTCP, which are characteristic of free-base and Zn(II) complexes of *meso*-substituted porphyrins [19,26]. These emission bands were assigned to the Q<sub>x</sub>(0-0) and Q<sub>x</sub>(0-1) transitions, which are typical of porphyrins. Similar results to those of the monomers were obtained for TCP-P and ZnTCP-P. Thus, the fluorescence emission properties of the porphyrin units were retained in the polymers. The  $\Phi_{\text{F}}$  values calculated for these compounds are indicated in Table 1. Slightly lower results were found for TCP-P and ZnTCP-P with respect to their corresponding constitutional monomers. The  $\Phi_{\text{F}}$  values are comparable to those previously reported for similar porphyrin derivatives [26]. From the absorption and fluorescence wavelength maxima of the Q<sub>x</sub>(0-0) bands, the Stokes shifts for the polymers were determined, giving values of 6 and 10 nm for TCP-P and ZnTCP-P, respectively. These Stokes shifts indicate that small structural changes occur between the ground state and the excited singlet state of the tetrapyrrolic macrocycle due to the rigidity of the structures. Therefore, the UV-visible absorption and fluorescence emission results confirm the polymerization of porphyrins as the constitutional component of the polymer conjugates.

### 3.4. Production of O<sub>2</sub>(<sup>1</sup>Δ<sub>g</sub>)

Photooxidation of DMA sensitized by TCP-P and ZnTCP-P was evaluated in DMF. In addition, the photodynamic effect induced by the polymers was compared with that of the monomers in the solution. The samples of the anthracene derivative and each PS were irradiated at 430 nm under aerobic conditions. The formation of the 9,10-endoperoxide derivative was explored following the changes in the UV-visible absorption spectra (Figure S3). The PSs showed negligible photobleaching during irradiation. The reaction was analyzed by the decrease in the absorbance of DMA at 378 nm [20]. Under these conditions, DMA decomposition exhibits pseudo-first-order kinetics with respect to substrate concentration (Figure 4). In Table 1 are shown the values of  $k_{\text{obs}}^{\text{DMA}}$  sensitized by these compounds. As can be seen, the rates of DMA decomposition induced by TCP-P and ZnTCP-P were approximately 1.2–1.3 times slower than those obtained for the monomers, indicating that porphyrin units retain their photodynamic activity in the polymer structures.

It was established that DMA, as a molecular probe, quenches O<sub>2</sub>(<sup>1</sup>Δ<sub>g</sub>) mainly by chemical reaction [28]. Thus, the kinetic data obtained for each PS were analyzed with respect to that of the reference (TCP) to determine the values of  $\Phi_{\Delta}$  [19]. As can be observed in Table 1, the  $\Phi_{\Delta}$  found for ZnTCP was slightly higher than that of TCP. However, this result is lower than that expected for Zn(II) *meso*-tetraphenylporphyrin derivatives [26,29]. The values of  $\Phi_{\Delta}$  for TCP-P and ZnTCP-P were slightly lower (~1.3 times) than those of the corresponding monomer in solution. In an earlier study, TCP and ZnTCP were electrochemically deposited, forming polymeric films on ITO electrodes [17]. However, these electrogenerated polymers on a surface showed a low photodynamic activity to produce O<sub>2</sub>(<sup>1</sup>Δ<sub>g</sub>). In these systems, the porphyrin units form a thin polymeric film that is only in contact with molecules near the surface. Furthermore, the presence of interactions between the tetrapyrrolic macrocycles in the hyperbranched film structure produces a decrease in the photodynamic effect [30]. In contrast, the polymers of the present work



were obtained in solution by an oxidative process. This procedure allows the application of these compounds dissolved in different media, improving the interaction with the surrounding microenvironment. Therefore, **TCP-P** and **ZnTCP-P** appear to be interesting photosensitizing materials suitable for inactivating bacteria.

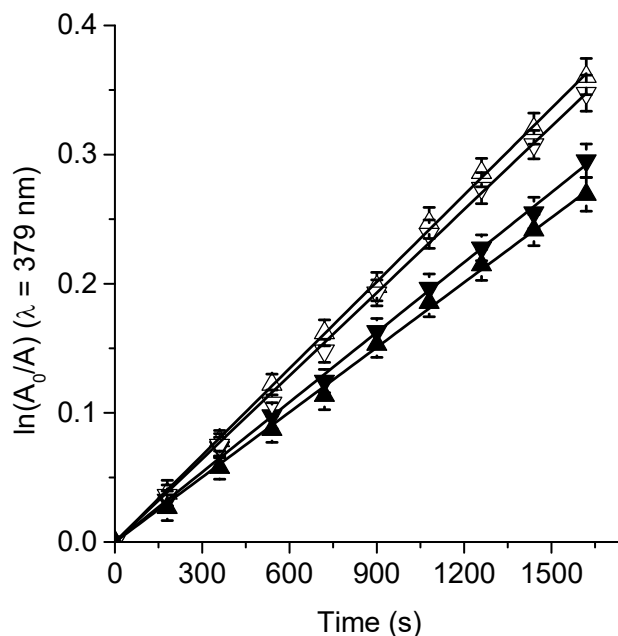


**Figure 4.** First-order plots for the photooxidation of DMA sensitized by **TCP** ( $\nabla$ ), **ZnTCP** ( $\Delta$ ), **TCP-P** ( $\blacktriangledown$ ) and **ZnTCP-P** ( $\blacktriangle$ ) in DMF,  $\lambda_{irr} = 430$  nm.

### 3.5. Photoinactivation of *S. aureus* Cell Suspensions

In order to establish the capacity of **TCP-P** and **ZnTCP-P** as antimicrobial PSs, the photodynamic activity induced by these polymers was evaluated to inactivate *S. aureus*. First, the viability of the cells after different irradiation periods was assessed in planktonic cells. A typical strain of Gram-positive MRSA was selected due to its ability to produce infections [4,5]. Thus, bacterial suspensions in PBS ( $10^4$  CFU/mL) were incubated with 2 or 4  $\mu$ M PSs for 30 min at 37 °C in the dark. Then, the bacterial cells were irradiated with white light for different times (10, 20, and 30 min). At these concentrations, dark controls of cells did not show any toxicity (Figure S4). Furthermore, the viability of *S. aureus* was not affected by irradiation of the cultures without the PS (Figure 5). Therefore, the death of the bacterial cells was due to the cytotoxic damage produced by the photodynamic action of the polymers. Figure 5A shows the survival of *S. aureus* treated with 2  $\mu$ M **TCP-P** and **ZnTCP-P** after different irradiation periods. The PDI was dependent on the polymer used and the period of exposure to white light. Both polymers produced photoinactivation of bacteria. **TCP-P** achieved a decrease in cell survival of approximately 3 logs after 30 min of irradiation, while **ZnTCP-P** produced a reduction of 2.8 logs. Mainly at shorter irradiation periods (10 and 20 min), **TCP-P** was slightly more effective than **ZnTCP-P**. Furthermore, as shown in Figure 5B, the photoinactivation of bacteria was investigated in cultures of *S. aureus* incubated with 4  $\mu$ M PS. Under this condition, **TCP-P** reached a 4-log reduction in the survival for *S. aureus* after an irradiation period of 20 min. This photokilling represents a reduction of bacterial cell survival greater than 99.99%. As expected, comparable results were found using **TCP-P** upon 30 min of irradiation. On the other hand, **ZnTCP-P** was less effective at all irradiation times, reaching a decrease of 3 logs upon 30 min of irradiation. For *S. aureus* cells incubated with **ZnTCP-P**, the dependence on concentration was lower, possibly due to the formation of aggregates in the aqueous medium as concentration increases.

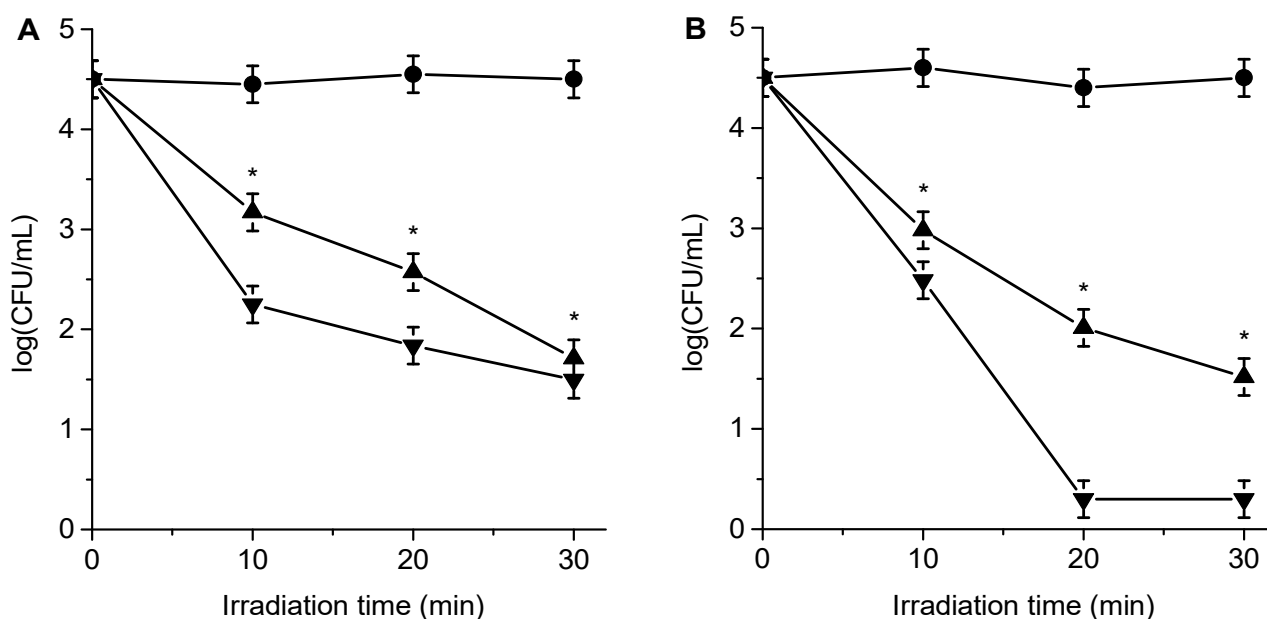


**Figure 5.** Survival curves of *S. aureus* ( $\sim 10^4$  CFU/mL) treated with (A) 2  $\mu$ M and (B) 4  $\mu$ M TCP-P (▼) and ZnTCP-P (▲) for 30 min at 37 °C in the dark and irradiated with white light for different times. Irradiated control culture without PS (●) (\* $p < 0.05$  compared with control).

In previous studies, photoactive polymers were investigated to inactivate microorganisms. Polymeric compounds were obtained from 2-hydroxyethyl methacrylate and porphyrin units [31]. The material containing the covalently bound tetrapyrrolic macrocycle was the most effective in killing bacteria. Furthermore, a conjugated polymer based on Zn(II) porphyrin was formed by the homocoupling reaction of terminal alkyne groups [15]. This compound was an effective PS able to eliminate *S. aureus* in bacterial suspensions. The polymers of the present work are poorly soluble in aqueous media. However, this lipophilic property may favor the interaction of the polymeric PS with *S. aureus* cells, increasing photoinactivation ability.

### 3.6. Photoinactivation of *S. aureus* on Surfaces

The photokilling activity induced by TCP-P and ZnTCP-P was assayed by examining individual bacteria using a fluorescence microscope. Therefore, *S. aureus* cells were adhered to the surface of a coverslip in a circular chamber, following the previously described methodology [21,32]. This experimental method was based on the presence of bacterial pili that help bacterial attachment to a surface [33]. Therefore, this approach represents a simplified instance of the first stage of biofilm formation [34]. Fluorescence images produced by PI were compared with phase contrast photographs to confirm the presence and position of bacteria on surfaces (Figure 6). After incubation of the individual *S. aureus* cells with 1  $\mu$ M PI for 15 min, bacteria were treated with 4  $\mu$ M PS in PBS for another 20 min in the dark. PI binds to DNA by intercalating between bases after cell membrane rupture. In an aqueous solution, PI presents a low red emission ( $\Phi_F \sim 0.01$ ). However, upon PI binding to DNA, this emission value can increase up to 30-fold [35]. Thus, this fluorophore was used as a cell death marker for the bacteria bound in the chamber [36].

For PDI tests at the single-bacterium level, *S. aureus* cells were irradiated with green light coming from the microscope source at different times. Figure 6 shows the progress in PDI therapy sensitized by PSs after different irradiation times between 0 and 30 min. Control experiments of cells irradiated in the absence of PS showed no significant cell damage after 30 min of irradiation (Figure S5). Photodamage of *S. aureus* cells sensitized by polymers was characterized by an increase in red fluorescence of the cell death marker (Figure 6). Under these experimental conditions, TCP-P and ZnTCP-P were able to produce

photoinactivation of bacterial cells. Upon 30 min of irradiation, an inactivation of 90% and 85% were reached for *S. aureus* cells adhered to the surface and treated with **TCP-P** and **ZnTCP-P**, respectively. In these experiments, the polymer formed by the free-base porphyrin was also slightly more effective than that containing the complex with Zn(II). In previous studies, similar photokilling results were found in *S. aureus* cells sensitized by porphyrins attached to magnetic nanoparticles [32]. In addition, several BODIPY derivatives were effective in eliminating *S. aureus* bound to a surface [21,37]. This approach was also established to determine the photoinactivating capacity of polymeric films of PSs deposited on a surface [30,38]. Therefore, these results indicate that **TCP-P** and **ZnTCP-P** were effective PSs in photoinactivating bacteria attached to surfaces.

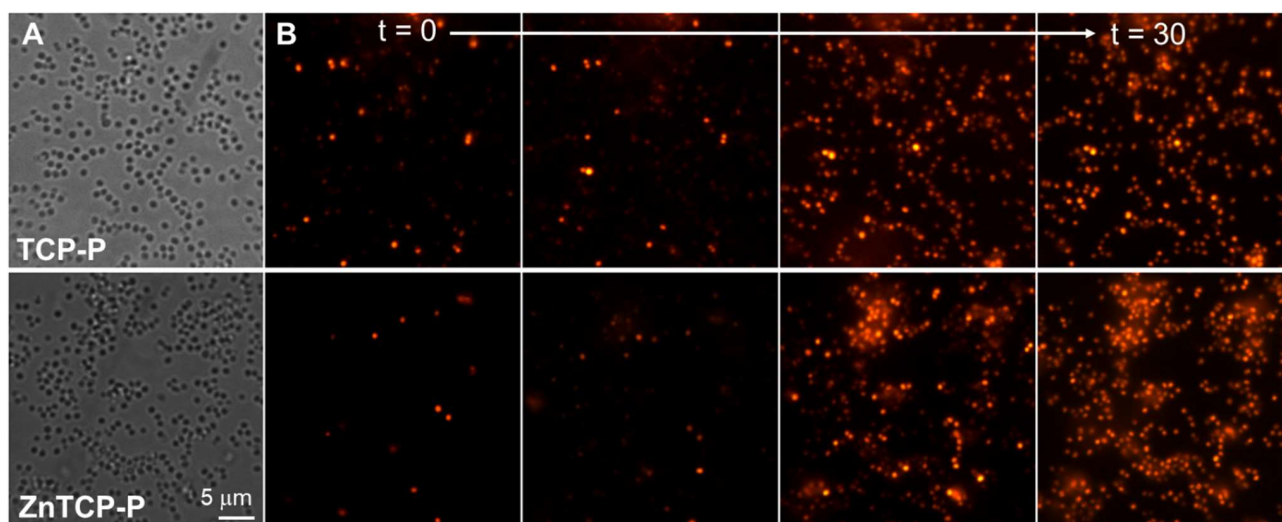


**Figure 6.** Microscopy images of *S. aureus* incubated with 4 μM PS for 20 min at 37 °C in the dark and then irradiated with green light for different times; column (A) cells under bright field; column (B) fluorescence emission of PI.

#### 4. Conclusions

Two polymeric compounds, **TCP-P** and **ZnTCP-P**, were synthesized by oxidative polymerization of the carbazole groups in high yields. This substituent has the ability to polymerize through the formation of the cationic radical. The solid material presented sizes of nanostructures with a rod shape. Small changes in the absorbance and fluorescence spectra of polymers indicate that the  $\pi$ - $\pi$  stacking between the constitutional porphyrins was hindered and only took place in a weak interaction. Moreover, the vibronic structure of these PSs remains almost unchanged upon excitation. These polymeric materials were able to produce efficiently  $O_2(^1\Delta_g)$  in solution. On the other hand, PDI investigations in bacterial cell suspensions showed that the photodynamic activity sensitized by these polymers allowed inactivated *S. aureus*. A reduction of 99.9% in cell survival was found for culture treated with 2 μM PS upon 30 min of irradiation. Doubling the **TCP-P** concentration, complete eradication of *S. aureus* cells was observed after 20 min of light. Under the same irradiation conditions, **TCP-P** was more efficient than **ZnTCP-P** against *S. aureus*. The lower inactivation induced by **ZnTCP-P** may be due to the formation of aggregates in aqueous media that precludes photodynamic activity. Furthermore, high photodamage induced by both polymers was observed at the single-bacterium level of *S. aureus* cells attached to a surface. The present study shows that these conjugated photodynamic polymers represent interesting antimicrobial agents to eradicate pathogens.

**Supplementary Materials:** The following supporting information can be downloaded at: <https://www.mdpi.com/article/10.3390/photochem2040057/s1>, Figure S1: Photographs of **TCP-P** in methanol and after centrifugation. Figure S2: UV-visible absorption spectra of oxidative polymerizations to obtain **TCP-P** and **ZnTCP-P** in DMF. Figure S3: Absorption spectral changes during the photooxidation of DMA sensitized by (A) **TCP**, (B) **ZnTCP**, (C) **TCP-P** and (D) **ZnTC-P** in DMF at different irradiation times ( $\Delta t = 180$  s),  $\lambda_{\text{irr}} = 430$  nm. Figure S4: Survival curves of *S. aureus* ( $\sim 10^4$  CFU/mL) treated with (A) 2  $\mu\text{M}$  and (B) 4  $\mu\text{M}$  **TCP-P** and **ZnTCP-P** for 30 min at 37 °C in the dark and incubated for different times in the dark. Figure S5: Microscopy images of *S. aureus* in the dark and then irradiated with green light for different times; column A: cells under bright field; columns B: fluorescence emission of PI.

**Author Contributions:** Conceptualization, M.B.B., S.C.S., M.E.P., J.E.D., M.E.M. and E.N.D.; methodology, M.B.B., S.C.S., M.E.P., J.E.D., M.E.M. and E.N.D.; validation, M.B.B., S.C.S., M.E.P., J.E.D., M.E.M. and E.N.D.; formal analysis, M.B.B., S.C.S. and M.E.P.; investigation, M.B.B., S.C.S. and M.E.P.; data curation, M.B.B., S.C.S., M.E.P. and J.E.D.; writing—original draft preparation, J.E.D., M.E.M. and E.N.D.; writing—review and editing, J.E.D., M.E.M. and E.N.D.; visualization, M.B.B., S.C.S., M.E.P., J.E.D., M.E.M. and E.N.D.; supervision, E.N.D.; project administration, E.N.D. All authors have read and agreed to the published version of the manuscript.

**Funding:** This research was funded by CONICET (PIP 2021-23 PIP 11220200101208CO) and ANPCYT (PICT-2019-02391).

**Institutional Review Board Statement:** Not applicable.

**Informed Consent Statement:** Not applicable.

**Data Availability Statement:** Not applicable.

**Acknowledgments:** This work was supported by CONICET (PIP 2021-23 PIP 11220200101208CO) and ANPCYT (PICT 2019- 02391). J.E.D., M.A.M.D. and E.N.D. are Scientific Members of CONICET. M.B.B., S.C.S. and M.E.P. thank CONICET for the research fellowship.

**Conflicts of Interest:** The authors declare no conflict of interest.

## References

1. Bassetti, S.; Tschudin-Sutter, S.; Egli, A.; Osthoff, M. Optimizing antibiotic therapies to reduce the risk of bacterial resistance. *Eur. J. Intern. Med.* **2022**, *99*, 7–12. [[CrossRef](#)] [[PubMed](#)]
2. Hassoun-Kheir, N.; Stabholz, Y.; Kreft, J.-U.; de la Cruz, R.; Romalde, J.L.; Nesme, J.; Sørensen, S.J.; Smets, B.F.; Graham, D.; Paul, M. Comparison of antibiotic-resistant bacteria and antibiotic resistance genes abundance in hospital and community wastewater: A systematic review. *Sci. Total Environ.* **2020**, *743*, 140804. [[CrossRef](#)] [[PubMed](#)]
3. Thomas, R.E.; Thomas, B.C.; Conly, J.; Lorenzetti, D. Cleaning and disinfecting surfaces in hospitals and long-term care facilities for reducing hospital- and facility-acquired bacterial and viral infections: A systematic review. *J. Hosp. Infect.* **2022**, *122*, 9–26. [[CrossRef](#)] [[PubMed](#)]
4. Shankar, N.; Soe, P.-M.; Tam, C.C. Prevalence and risk of acquisition of methicillin-resistant *Staphylococcus aureus* among households: A systematic review. *Int. J. Infect. Dis.* **2020**, *92*, 105–113. [[CrossRef](#)]
5. Liu, W.-T.; Chen, E.-Z.; Yang, L.; Peng, C.; Wang, Q.; Xu, Z.; Chen, D.-Q. Emerging resistance mechanisms for 4 types of common anti-MRSA antibiotics in *Staphylococcus aureus*: A comprehensive review. *Microb. Pathog.* **2021**, *156*, 104915. [[CrossRef](#)]
6. Lin, D.; Ou, Q.; Lin, J.; Peng, Y.; Yao, Z. A meta-analysis of the rates of *Staphylococcus aureus* and methicillin-resistant *S. aureus* contamination on the surfaces of environmental objects that health care workers frequently touch. *Am. J. Infect. Control* **2017**, *45*, 421–429. [[CrossRef](#)]
7. Ghosh, C.; Sarkar, P.; Issa, R.; Haldar, J. Alternatives to conventional antibiotics in the era of antimicrobial resistance. *Trends Microbiol.* **2019**, *27*, 323–338. [[CrossRef](#)]
8. Youf, R.; Müller, M.; Balasini, A.; Thétiot, F.; Müller, M.; Hascoët, A.; Jonas, U.; Schönherr, H.; Lemerrier, G.; Montier, T.; et al. Antimicrobial photodynamic therapy: Latest developments with a focus on combinatory strategies. *Pharmaceutics* **2021**, *13*, 1995. [[CrossRef](#)]
9. Durantini, A.M.; Heredia, D.A.; Durantini, J.E.; Durantini, E.N. BODIPYs to the rescue: Potential applications in photodynamic inactivation. *Eur. J. Med. Chem.* **2018**, *144*, 651–661. [[CrossRef](#)]
10. Ogilby, P.R. Singlet oxygen: There is still something new under the sun, and it is better than ever. *Photochem. Photobiol. Sci.* **2010**, *9*, 1543–1560. [[CrossRef](#)]
11. Kashaf, N.; Hamblin, M.R. Can microbial cells develop resistance to oxidative stress in antimicrobial photodynamic inactivation? *Drug Resist. Updates* **2017**, *31*, 31–42. [[CrossRef](#)] [[PubMed](#)]



12. Alves, E.; Faustino, M.A.F.; Neves, M.G.P.M.S.; Cunha, Â.; Nadais, H.; Almeida, A. Potential applications of porphyrins in photodynamic inactivation beyond the medical scope. *J. Photochem. Photobiol. C Photochem. Rev.* **2015**, *22*, 34–57. [[CrossRef](#)]
13. Sobotta, L.; Skupin-Mrugalska, P.; Piskorz, J.; Mielcarek, J. Porphyrinoid photosensitizers mediated photodynamic inactivation against bacteria. *Eur. J. Med. Chem.* **2019**, *175*, 72–106. [[CrossRef](#)] [[PubMed](#)]
14. Tian, J.; Zhang, W. Synthesis, self-assembly and applications of functional polymers based on porphyrins. *Prog. Polym. Sci.* **2019**, *95*, 65–117. [[CrossRef](#)]
15. Santamarina, S.C.; Heredia, D.A.; Durantini, A.M.; Durantini, E.N. Antimicrobial photosensitizing material based on conjugated Zn(II) porphyrins. *Antibiotics* **2022**, *11*, 91. [[CrossRef](#)]
16. Durantini, J.; Otero, L.; Funes, M.; Durantini, E.N.; Fungo, F.; Gervaldo, M. Electrochemical oxidation-induced polymerization of 5,10,15,20-tetrakis[3-(*N*-ethylcarbazoyl)] porphyrin. Formation and characterization of a novel electroactive porphyrin thin film. *Electrochim. Acta* **2011**, *56*, 4126–4134. [[CrossRef](#)]
17. Ballatore, M.B.; Durantini, J.; Gsponer, N.S.; Suarez, M.B.; Gervaldo, M.; Otero, L.; Spesia, M.B.; Milanesio, M.E.; Durantini, E.N. Photodynamic inactivation of bacteria using novel electrogenerated porphyrin-fullerene C60 polymeric films. *Environ. Sci. Technol.* **2015**, *49*, 7456–7463. [[CrossRef](#)]
18. Siove, A.; Adès, D. Synthesis by oxidative polymerization with FeCl<sub>3</sub> of a fully aromatic twisted poly(3,6-carbazole) with a blue-violet luminescence. *Polymer* **2004**, *45*, 4045–4049. [[CrossRef](#)]
19. Ballatore, M.B.; Spesia, M.B.; Milanesio, M.E.; Durantini, E.N. Synthesis, spectroscopic properties and photodynamic activity of porphyrin-fullerene C60 dyads with application in the photodynamic inactivation of *Staphylococcus aureus*. *Eur. J. Med. Chem.* **2014**, *83*, 685–694. [[CrossRef](#)]
20. Pérez, M.E.; Durantini, J.E.; Reynoso, E.; Alvarez, M.G.; Milanesio, M.E.; Durantini, E.N. Porphyrin-schiff base conjugates bearing basic amino groups as antimicrobial phototherapeutic agents. *Molecules* **2021**, *26*, 5877. [[CrossRef](#)]
21. Martínez, S.R.; Palacios, Y.B.; Heredia, D.A.; Agazzi, M.L.; Durantini, A.M. Phenotypic resistance in photodynamic inactivation unravelled at the single bacterium level. *ACS Infect. Dis.* **2019**, *5*, 1624–1633. [[CrossRef](#)] [[PubMed](#)]
22. Feng, L.-J.; Chen, Q.; Zhu, J.-H.; Liu, D.-P.; Zhao, Y.-C.; Han, B.-H. Adsorption performance and catalytic activity of porous conjugated polyporphyrins via carbazolebased oxidative coupling polymerization. *Polym. Chem.* **2014**, *5*, 3081–3088. [[CrossRef](#)]
23. Bekkar, F.; Bettahar, F.; Moreno, I.; Meghabar, R.; Hamadouche, M.; Hernández, E.; Vilas-Vilela, J.L.; Ruiz-Rubio, L. Polycarbazole and its derivatives: Synthesis and applications. A review of the last 10 years. *Polymers* **2020**, *12*, 2227. [[CrossRef](#)] [[PubMed](#)]
24. Wang, N.; Li, Y.; Lu, F.; Liu, Y.; He, X.; Jiang, L.; Zhuang, J.; Li, X.; Li, Y.; Wang, S.; et al. Fabrication of novel conjugated polymer nanostructure: Porphyrins and fullerenes conjugately linked to the polyacetylene backbone as pendant groups. *J. Polym. Sci. Part A Polym. Chem.* **2005**, *43*, 2851–2861. [[CrossRef](#)]
25. Maximiano, R.V.; Piovesan, E.; Zílio, S.C.; Machado, A.E.H.; de Paula, R.; Cavaleiro, J.A.S.; Borissevitch, I.E.; Ito, A.S.; Gonçalves, P.J.; Barbosa Neto, N.M. Excited-state absorption investigation of a cationic porphyrin derivative. *J. Photochem. Photobiol. A Chem.* **2010**, *214*, 115–120. [[CrossRef](#)]
26. Scalise, I.; Durantini, E.N. Photodynamic effect of metallo 5-(4-carboxyphenyl)-10,15,20-tris(4-methylphenyl) porphyrins in biomimetic AOT reverse micelles containing urease. *J. Photochem. Photobiol. A Chem.* **2004**, *162*, 105–113. [[CrossRef](#)]
27. McDonald, A.R.; Franssen, N.; van Klink, G.P.M.; van Koten, G. ‘Click’ silica immobilisation of metallo-porphyrin complexes and their application in epoxidation catalysis. *J. Organomet. Chem.* **2009**, *694*, 2153–2162. [[CrossRef](#)]
28. Gomes, A.; Fernandes, E.; Lima, J.L.F.C. Fluorescence probes used for detection of reactive oxygen species. *J. Biochem. Biophys. Methods* **2005**, *65*, 45–80. [[CrossRef](#)]
29. Milanesio, M.E.; Alvarez, M.G.; Bertolotti, S.G.; Durantini, E.N. Photophysical characterization and photodynamic activity of metallo 5-(4-(trimethylammonium) phenyl)-10,15,20-tris(2,4,6-trimethoxyphenyl) porphyrin in homogeneous and biomimetic media. *Photochem. Photobiol. Sci.* **2008**, *7*, 963–972. [[CrossRef](#)]
30. Heredia, D.A.; Martínez, S.R.; Durantini, A.M.; Pérez, M.E.; Mangione, M.I.; Durantini, J.E.; Gervaldo, M.A.; Otero, L.A.; Durantini, E.N. Antimicrobial photodynamic polymeric films bearing bis-carbazole triphenylamine end-capped dendrimeric Zn (II) porphyrin. *ACS Appl. Mater. Interfaces* **2019**, *11*, 27574–27587. [[CrossRef](#)]
31. Castro, K.A.D.F.; Moura, N.M.M.; Simões, M.M.Q.; Cavaleiro, J.A.S.; Faustino, M.A.F.; Cunha, Â.; Almeida Paz, F.A.; Mendes, R.F.; Almeida, A.; Freire, C.S.R.; et al. Synthesis and characterization of photoactive porphyrin and poly (2-hydroxyethyl methacrylate) based materials with bactericidal properties. *Appl. Mater. Today* **2019**, *16*, 332–341. [[CrossRef](#)]
32. Scanone, A.C.; Gsponer, N.S.; Alvarez, M.G.; Heredia, D.A.; Durantini, A.M.; Durantini, E.N. Magnetic nanoplatforms for in situ modification of macromolecules: Synthesis, characterization, and photoinactivating power of cationic nanoimman-porphyrin conjugates. *ACS Appl. Bio Mater.* **2020**, *3*, 5930–5940. [[CrossRef](#)] [[PubMed](#)]
33. Danne, C.; Dramsi, S. Pili of Gram-positive bacteria: Roles in host colonization. *Res. Microbiol.* **2012**, *163*, 645–658. [[CrossRef](#)] [[PubMed](#)]
34. Guzmán-Soto, I.; McTiernan, C.; Gonzalez-Gomez, M.; Ross, A.; Gupta, K.; Suuronen, E.J.; Mah, T.-F.; Griffith, M.; Alarcon, E.I. Mimicking biofilm formation and development: Recent progress in in vitro and in vivo biofilm models. *iScience* **2021**, *24*, 102443. [[CrossRef](#)] [[PubMed](#)]
35. Samanta, A.; Paul, B.K.; Guchhait, N. Photophysics of DNA staining dye propidium iodide encapsulated in bio-mimetic micelle and genomic fish sperm DNA. *J. Photochem. Photobiol. B Biol.* **2012**, *109*, 58–67. [[CrossRef](#)] [[PubMed](#)]



36. Duedu, K.O.; French, C.E. Two-colour fluorescence fluorimetric analysis for direct quantification of bacteria and its application in monitoring bacterial growth in cellulose degradation systems. *J. Microbiol. Methods* **2017**, *135*, 85–92. [[CrossRef](#)] [[PubMed](#)]
37. Scanone, A.C.; Santamarina, S.C.; Heredia, D.A.; Durantini, E.N.; Durantini, A.M. Functionalized magnetic nanoparticles with BODIPYs for bioimaging and antimicrobial therapy applications. *ACS Appl. Bio Mater.* **2020**, *3*, 1061–1070. [[CrossRef](#)]
38. Baigorria, E.; Durantini, J.E.; Martínez, S.R.; Milanesio, M.E.; Palacios, Y.B.; Durantini, A.M. Potentiation effect of iodine species on the antimicrobial capability of surfaces coated with electroactive phthalocyanines. *ACS Appl. Bio Mater.* **2021**, *4*, 8559–8570. [[CrossRef](#)]